

A Novel Enolase-1 Antibody Targets Multiple Interacting Players in the Tumor Microenvironment of Advanced Prostate Cancer

Mao-Lin Chen, Ta-Tung Yuan, Chi-Fen Chuang, Yung-Tsang Huang, I-Che Chung, and Wei-Ching Huang



ABSTRACT

Prostate cancer is one of the most common causes of cancer death in men worldwide, and the treatment options are limited for patients with advanced stages of prostate cancer. Upon oncogenic or inflammatory stimulation, tumor cells or immune cells express cell surface enolase-1 (ENO1) as plasminogen receptor to facilitate their migration via plasmin activation. Little is known about the roles of ENO1 in prostate cancer, especially in the tumor microenvironment (TME). We hypothesized that targeting surface ENO1 with specific mAbs would exert multifactorial therapeutic potentials against prostate cancer. *In vivo*, we showed ENO1 mAb (HuL227) reduced the growth of subcutaneous PC-3 xenograft, monocytes recruitment, and intratumoral angiogenesis. In a PC-3 intratibial implantation model, HuL227 reduced tumor growth

and osteoclast activation in the bone. To investigate the anti-tumor mechanism of ENO1 mAb, we found that blocking surface ENO1 significantly reduced VEGF-A-induced tube formation of endothelial cells *in vitro*. Furthermore, HuL227 inhibited inflammation-enhanced osteoclasts activity and the secretion of invasion-related cytokines CCL2 and TGF β from osteoclasts. In addition, inflammation-induced migration and chemotaxis of androgen-independent prostate cancer cells were dose-dependently inhibited by HuL227. In summary, we showed that, ENO1 mAb targets multiple TME niches involved in prostate cancer progression and bone metastasis via a plasmin-related mechanism, which may provide a novel immunotherapy approach for men with advanced prostate cancer.

Introduction

In 2020, cancer statistics expected that in the United States, prostate cancer would be the most common type of cancer in men, in which prostate cancer alone accounts for more than one in five new diagnoses (1). Furthermore, prostate cancer will be responsible for 10% of estimated cancer-related deaths, second to lung and bronchus cancer of 23% in men (1). Early-stage prostate cancer can often be successfully treated with active surveillance, surgery, radiation, or androgen-deprivation therapy (ADT). However, development of resistance to ADT leads to progression of castration-resistant prostate cancer (CRPC; ref. 2). The risk of death is highest among men who further develop metastatic CRPC (mCRPC). Bone is a preferential metastatic site for prostate cancer cells. Once patients with prostate cancer develop skeletal metastases, the advanced tumor is currently incurable, and there remains a high demand for treatment options to improve the outcome of patients with mCRPC.

The tumor microenvironment (TME), which is created by tumor and tumor stroma, plays critical roles in prostate cancer progression and metastasis. In the TME, both tumor and tumor stroma secrete chemokines and cytokines that can influence the composition of

immune cell infiltrates, tumor growth, angiogenesis, and metastasis (3). In addition, the “tumor-reactive stroma,” consisting of a mixture of fibroblasts, vasculature, lymphocytes, and macrophages, contributes to an inflammatory cytokine-rich TME with soluble factors, including TNF α , TGF β , and VEGF (4, 5). During prostate cancer metastasis, TGF β and VEGF are potent mediators of epithelial-mesenchymal transition (EMT) and angiogenesis, respectively. Men with prostate cancer often develop bone metastasis if not effectively contained. The interaction between prostate cancer and bone cells (osteoclasts, osteoblasts, and osteocytes) results in increased osteolysis and osteosclerosis, leading to bone pain and pathologic fractures in patients with prostate cancer (6). Emerging evidence reveals that the osteoblastic niche is a potential area for prostate cancer bone metastases (7). In the meantime, the osteoclast-targeting therapy with bisphosphonate or zoledronic acid reduced bone complications in patients with prostate cancer with bone metastases after receiving ADT (8). Therefore, considerations of homeostatic balance between osteoclast-mediated bone resorption and osteoblast-mediated bone formation is critical for developing treatment of bone metastases in patients with prostate cancer.

Plasminogen and plasmin play important roles in many essential biological processes such as cell migration, tissue remodeling, wound healing, angiogenesis, inflammation, and cancer metastasis (9). Enolase-1 (ENO1) or alpha-enolase is one of the plasminogen receptors, in addition to its intracellular function in glycolysis, when translocated onto cell surface from cytosol (10). Plasminogen is tethered to the cell surface by binding to ENO1, which further activates plasmin generation. Cells armed with plasmin acquire ability of pericellular proteolysis to facilitate transmigration and degradation of basement membrane or extracellular matrix (ECM; ref. 11). In inflammatory diseases such as pneumonia and rheumatoid arthritis, increased surface ENO1 expression on blood monocytes was found in patients (10, 12). In cancers, surface ENO1 overexpression has been associated with breast, lung, and pancreatic neoplasms (13). Blockade of cell surface ENO1

HuniLife Biotechnology Inc., Taiwan.

Corresponding Authors: Wei-Ching Huang, Department of Research and Development, HuniLife Biotechnology Inc., Rm. 1, 6F, No.308, Sec. 1, Neihu Road, Neihu District, Taipei City 114, Taiwan. Phone: 8862-2657-9668; Fax: 8862-2657-9669; E-mail: wchuang@hunilife.com; and Ta-Tung Yuan, tyuan@hunilife.com

Mol Cancer Ther 2022;21:1337-47

doi: 10.1158/1535-7163.MCT-21-0285

This open access article is distributed under the Creative Commons Attribution-NonCommercial-NoDerivatives 4.0 International (CC BY-NC-ND 4.0) license.

©2022 The Authors; Published by the American Association for Cancer Research

with anti-ENO1 antibodies thus has been shown in pancreatic and lung cancer as an effective anti-invasiveness/metastasis strategy (14, 15). However, little is known about the roles of surface ENO1 in prostate cancer, and no current therapeutic strategy is developed to target ENO1. Indirect evidence has shown that a novel ENO1-targeting peptide by which the antitumor activity of liposomal-delivered doxorubicin was significantly improved in prostate tumor-bearing mice (16). Another study reported that, in response to estrogen stimulation, the stromal cells of prostate cancer would secrete ENO1 to facilitate prostate cancer cell migration via the plasminogen/plasmin system (17). Although there is limited evidence to link surface ENO1 and prostate cancer, it is intriguing to speculate that ENO1 could play important roles in prostate cancer advancing to bone, based on the following observations. First, ENO1 is functionally expressed on the surface of prostate cancer cells, monocytes, osteoclasts, and endothelium cells in pathogenic situation. Second, generation of plasmin via the plasminogen/ENO1 axis on the above-mentioned cells enables their journey between prostate and bone.

Here we described HuL227, a first-in-class humanized ENO1 mAb, possessing a set of novel properties to target the important players of prostate cancer and bone metastasis. In addition to inhibiting the migration of prostate cancer cells via blocking the ENO1/plasmin axis, HuL227 also regulates TME via suppression of monocyte recruitment, angiogenesis, and the proinvasiveness activities of osteoclasts. These differentiative properties of ENO1 mAb will be of potential to provide a novel therapeutic strategy for treating patients with mCRPC.

Materials and Methods

Cell culture and reagents

The human prostate cancer cell lines LNCap (ATCC No. CRL-1740, RRID: CVCL_1379), androgen-dependent, and PC-3 (ATCC No. CRL-1435, RRID: CVCL_0035), androgen-independent, and mouse macrophage cell line Raw264.7 (ATCC No. TIB71, RRID: CVCL_0493) were obtained from and authenticated by the American Type Culture Collection (ATCC). Another androgen-independent human prostate cancer cell line DU145 (BCRC No. 60348, RRID: CVCL_0105) and human monocytic cell line THP-1 (BCRC No. 60430, RRID: CVCL_0006) were obtained from Bioresource Collection and Research Center (BCRC) and performed short tandem repeat (STR)-PCR profile at BCRC. Human Umbilical Vein Endothelial Cells (HUVECs; No. SC-8000) were from ScienCell Research Laboratories and used within 15 population doublings. LNCap, PC-3, and THP-1 were grown in RPMI-1640 (Gibco, Life Technologies), DU145 was grown in minimum essential medium (MEM; Gibco), and Raw264.7 was grown in DMEM. The cell lines were used within 2 months after thawing or within 25 passages. All the culture medium was supplemented with 10% FBS (Gibco) and 50 U/mL penicillin-streptomycin (Gibco), while DU145 required extra supplements containing 10% sodium pyruvate (Gibco) and 10% nonessential amino acids (NEAAs; Gibco). The culture medium for Raw264.7 was changed to osteoclast differentiation medium MEM α containing 10% FBS, 50 U/mL penicillin-streptomycin, and 10% Gluta-MAX (Gibco). HUVEC was cultured in endothelial cell medium (No. SC-1001, ScienCell) on a fibronectin-coated culture vessel (No. SC-8248, ScienCell; 2 μ g/cm²). All cells were maintained at 37°C in a 5% CO₂ humidified atmosphere and tested negative for *Mycoplasma* (BSMP-101, BIOMart) throughout the study. Lipopolysaccharide (LPS; No. L2360) was purchased from Sigma, and plasmin inhibitor tranexamic acid (TXA; No. T1810000) was from European Pharmacopoeia. Recombinant proteins of human TNF α (No. 300-01A), CCL2 (No. 300-04), TGF β

(No. 100-21), VEGF-A (No. 100-20), mouse RANKL (No. 315-11), and TNF α (No. 315-01A) were purchased from PeproTech. Matrigel (No. 356231) was from Corning.

Antibodies

HuL227 is a humanized derivative of the murine parental mAbs, EN10, specific for binding to ENO1 at a subnanomolar concentration and produced in Chinese hamster ovary (CHO) cells. EN10 was further described in PCT/US2013/076877, SEQ ID No. 1 (heavy chain), SEQ ID No. 2 (light chain), and SEQ ID No. 49 (epitope). The humanized variable regions of HuL227 are composed of mouse-derived EN10 complementarity determining regions (CDRs) engrafted into the ImMunoGeneTics (IMGT)-framework regions, which were then fused with the constant region of human IgG1 (hIgG1). The humanized IMGT-variable regions of both light chain and heavy chains were directly generated by nucleotide synthesis. HuL227 is cross-reactive to both human and mouse ENO1, but not binding to ENO2 and ENO3. HIG1 antibodies (No. HG1K) were purchased from Sino Biological and used as isotype control.

Animal studies

All animal studies were conducted in accordance with protocols approved by the Institutional Animal Care and Use Committee (IACUC) of TFBS Bioscience (IACUC protocol No. 2020-SH-018) or Tri-Neo Biotechnology (IACUC protocol No. 2020-SH-011). For PC-3 subcutaneous xenograft models (16), male 4- to 6-week-old BALB/c nude (*nu/nu*) mice were used (Lasco Co., Ltd.). Before inoculation, PC-3 cells were washed with PBS and resuspended with PBS and Matrigel at 1:1 for a final concentration of 10⁷ cells/mL. Cells (10⁶/100 μ L) were implanted subcutaneously into the right flank of mice. HuL227 was dosed by intraperitoneal injection. For PC-3 bone metastasis xenograft model (18), intratibial injection of PC-3 cells at 2 \times 10⁵ cells/40- μ L PBS was performed for each male 6- to 8-week-old NOD/SCID mouse (Lasco Co., Ltd.). HuL227 was dosed by intravenous injection. For both models, after 3 days of implantation, the mice were randomized to control and treatment groups, which were administrated with PBS (5 mL/kg) as vehicle control or ENO1 mAb HuL227 (30 mg/kg), respectively. The dosing and body weight measurement were performed twice per week. The volume of subcutaneous tumor was determined according to the formula: tumor volume = shorter diameter² \times longer diameter/2. In the bone metastasis model, Cat K 680 FAST contrast medium (No. NEV11000, PerkinElmer) was injected intravenously on day 15 and day 22 to detect osteoclast activity in the proximal tibia by using *in vivo* Fluorescence Molecular Tomography (FMT) imaging (FMT4000 system, PerkinElmer). Similarly, MIMPence 750 FAST contrast medium (No. NEV10168, PerkinElmer) was injected intravenously on day 27 to detect the growth of intratibial tumor by FMT imaging.

Immunofluorescence staining

For surface ENO1 staining, cells grown on 4-well glass slides were fixed in fixation buffer (No. 420801, Biolegend) for 15 minutes at 4°C, blocked in 0.1% bovine serum albumin (BSA) for 1 hour, and incubated with anti-ENO1 primary antibody (No. H00002023-M01, Abnova) for 1 hour at room temperature. After a brief wash with PBS, slides were incubated for 1 hour at room temperature with Alexa Fluor 488 conjugated goat anti-mouse IgG secondary antibody (A32723, Invitrogen). Nonbound antibodies were washed, and cell nuclei were stained with DAPI (No. D-9542, Sigma) for 5 to 10 minutes. After washing once with PBS, slides were mounted with Fluoromount-G (No. 0100-01, Bio Pioneer). Images were acquired using a Nikon

microscope (Japan). The subcutaneous tumor xenografts were excised and embed in OCT (Tissue-Tek; Sakura Finetek) by using liquid nitrogen, and the snap-frozen blocks were stored at -80°C for further processing. Frozen tissue sections (14 μm) were prepared, air-dried, and fixed in formalin for 10 minutes at room temperature. Slides were blocked for 1 hour in 2% BSA/0.3% TritonX-100 and then incubated with primary antibodies against CCR2 (No. ab273050, Abcam) or CD31 (No. ab28364, Abcam) overnight at 4°C . Following washing, slides were incubated for 2 hours at room temperature with secondary antibodies (Invitrogen), nonbound antibodies were washed, and cell nuclei were stained with DAPI (No. D-9542, Sigma) for 5 to 10 minutes. After a brief wash in PBS, stained sections were mounted with ProLong Gold antifade reagent (No. P36930, Invitrogen). Images were acquired using a Carl Zeiss microscope (Germany).

Endothelial cell tube formation assay

HUVECs were seeded at 10^4 cells/well on Matrigel-coated 96-well plate and stimulated with 25 ng/mL VEGF-A in the absence or presence of various concentrations of HuL227, 10 $\mu\text{g}/\text{mL}$ control hIgG1, or 10 mmol/L TXA. Tubes were allowed to form for 24 hours and quantified manually by counting the nodes in two random fields per well under light microscopy.

Migration and chemotaxis assays

For migration assay, after treated with LPS, TNF α , TGF β for 4 hours, 10^5 cells were resuspended in medium supplemented with 2% FBS in the absence or presence of various concentrations of HuL227, 10 $\mu\text{g}/\text{mL}$ control hIgG1, or 10 mmol/L TXA. After adding 900 μL of medium containing 10% FBS to the bottom well, the coating-free insert (8 $\mu\text{mol}/\text{L}$ pores; Corning) was placed in the bottom well and seeded with the treated cells. The cells were allowed to migrate at 37°C for 18 hour. The remaining cells on the upper part of the insert were removed by gently wiping with a cotton swab. The cells on the lower side of the insert were fixed with methanol for 10 minutes, followed by staining with 1% crystal violet for an additional 2 hours or overnight. The insert was gently washed with PBS and dried. The cells were counted under a microscope. Five views in a single well were randomly selected and counted for the cell numbers. For chemotaxis assay, serum-free medium was used, and the bottom wells were supplemented with CCL2 as chemoattractant.

Fibrinolytic assay

Cells were treated with indicated stimuli for 4 hours, washed twice with PBS, resuspended in PBS at 10^6 cells/mL, and preincubated with 30 $\mu\text{mol}/\text{L}$ human Glu-PLG (No. 528180-1MGCN, Sigma) in the absence or presence of various concentration of HuL227 or control hIgG1 at 37°C for 1 hour. After incubation, the cells were washed with PBS three times and resuspended in 100- μL PBS. Tissue plasminogen activator (tPA) at a concentration of 1.5 nmol/L (No. 612200, Sigma) and 0.1 mmol/L plasmin substrate Chromogenix S-2251 (No. S820332, Diapharma) were added to the cells and incubated at 37°C for 2.5 hours. The plasmin activity was determined by measurement of the absorbance at 405 nm.

Cytokine ELISA

Raw 264.7-derived osteoclasts were treated with 20 ng/mL TNF α in the absence or presence of various concentrations of HuL227, 10 $\mu\text{g}/\text{mL}$ control hIgG1, or 10 mmol/L TXA for 24 hours. Cell supernatant was collected by centrifugation at 3,000 rpm for 5 minutes and stored at -20°C . Measurement of cytokines was performed using ELISA kits following the manufacturer's instructions. ELISA kits of mouse CCL2

(No. ARG80120) and mouse TGF β (No. ARG80101) were purchased from Arigo biolaboratories.

Osteoclast differentiation from Raw264.7 cells

Raw264.7 cells were seeded at 10^4 per well in 24-well plates in differentiation medium, prestimulated with 20 ng/mL TNF α for 4 hours, and soluble RANKL (30 ng/mL) was added in the absence or presence of various concentrations of HuL227, 10 $\mu\text{g}/\text{mL}$ control hIgG1, or 10 mmol/L TXA for 7 days. The cells were then fixed and stained with a tartrate-resistant acid phosphatase (TRAP) staining kit (No. 387-A, Sigma), and TRAP-positive staining cells (multinuclear cells with >3 nuclei) were considered as osteoclasts.

qRT-PCR

Raw264.7 was pretreated with 20 ng/mL TNF α for 4 hours and treated with 30 ng/mL RANKL in the absence or presence of various concentrations of HuL227, 10 $\mu\text{g}/\text{mL}$ control hIgG1, or 10 mmol/L TXA for 96 hours. Total RNA of the treated cells was extracted using NucleoZOL (No. 740404.200, MACHEREY-NAGEL), according to the manufacturer's instructions. The cDNA synthesis and real-time PCR were performed using KAPA SYBR FAST qPCR Master Mix (No. KK4603, Kapa Biosystems), following the manufacturer's instructions. The primers used for PCR were NFTA1 F-5'-CAACGCCCTGACCACCGATAG-3', R-5'-GGGAAGTCAGAAAGTGGGTGGA-3', Cathepsin K F-5'-TGTATAACGCCACGGCAAAA-3', R-5'-GGTTCACATTATCACGGTCACA-3', as well as GAPDH F-5'-TGA-GGCCGGTGCTGAGTATGTGCG-3', and R-5'-CCACAGTCTCTG-GGTGGCAGTG-3'. Target genes mRNA expression levels were calculated by relative quantification (2- $\Delta\Delta\text{Ct}$) method. Experiments were performed in triplicate.

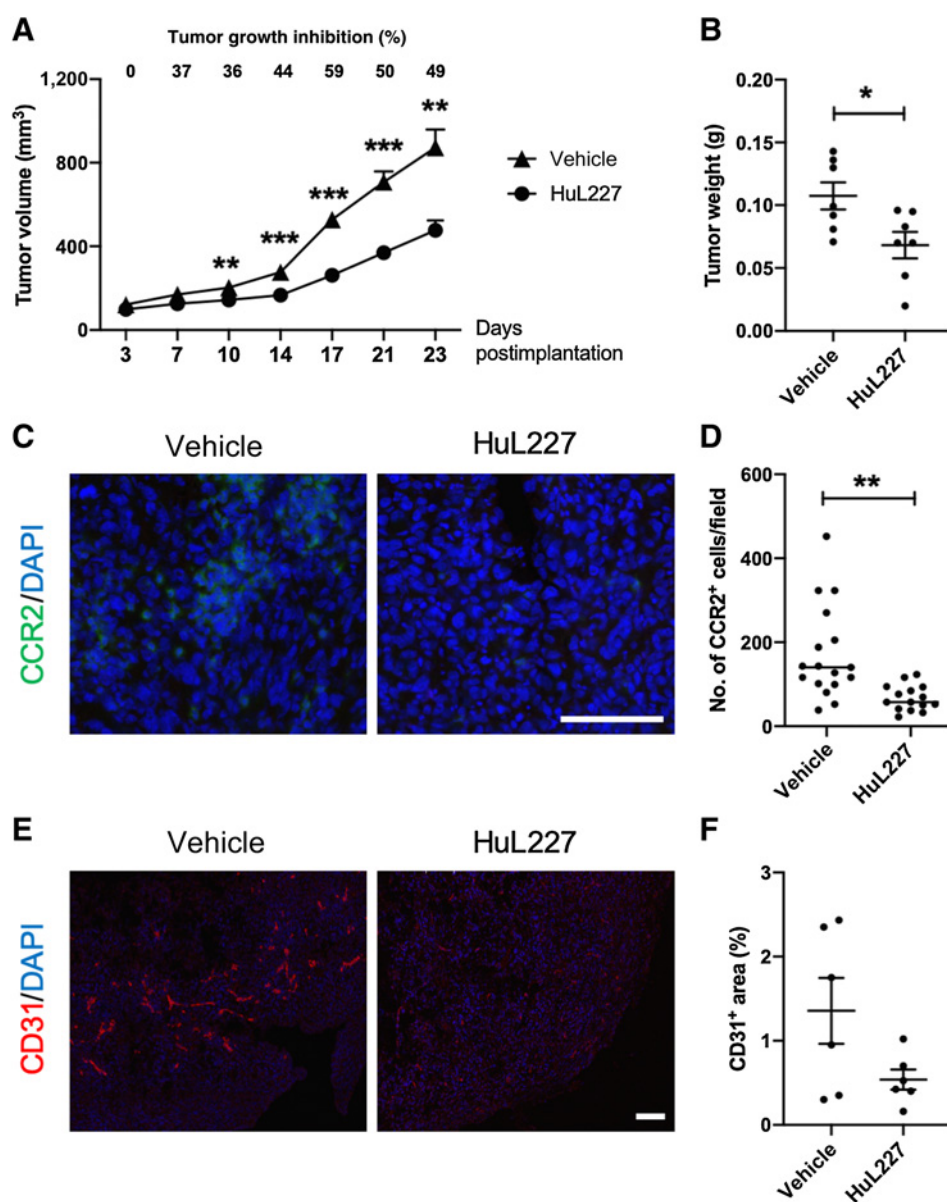
Statistical analysis

Results were shown as the mean \pm SD or mean \pm SEM. Data analysis was performed using GraphPad Prism 8. The Student *t* test was performed to compare the significance of the differences between two groups. Significant results were determined and indicated as * or #, $P < 0.05$; ** or ##, $P < 0.01$; and *** or ###, $P < 0.001$.

Results

ENO1 mAb HuL227 attenuates tumor growth, recruitment of CCR2⁺ inflammatory monocytes, and angiogenesis in the PC-3 subcutaneous xenograft model

Although targeting surface ENO1 is shown to inhibit tumor invasiveness and metastasis (14, 15), little is known regarding its roles in TME. Modulation of TME by ENO1 in prostate cancer has been implicated in previous study (17); we also found overexpression of ENO1 in the advanced grade of human prostate cancer tissues (Supplementary Fig. S1). Here, we used a PC-3 subcutaneous xenograft model to evaluate the therapeutic effects of a first-in-class ENO1 mAb HuL227. After dosing with HuL227 twice a week, we observed significant suppression of tumor growth measured by tumor volume (Fig. 1A) or tumor weight (Fig. 1B). Consistent results were also obtained in the DU145 subcutaneous xenograft model (Supplementary Fig. S2). Because HuL227 possesses a modest inhibitory effect on the proliferation of PC-3 and DU145 cells *in vitro* (Supplementary Fig. S3), we hypothesized that HuL227 could also regulate TME. In the excised tumors of PC-3 graft, we examined the expression of Ki-67 for proliferation (Supplementary Fig. S4A), F4/80 for tumor-associated macrophages (TAMs; Supplementary Fig. S4B), CCR2 for infiltrated inflammatory monocytes (Fig. 1C and D), and CD31 for intratumoral

**Figure 1.**

Anti-ENO1 mAb HuL227 attenuates tumor growth and angiogenesis in a prostate cancer PC-3 subcutaneous xenograft model. Male nude mice were subcutaneously implanted with PC-3 for 3 days, randomized, and dosed with 30 mg/kg HuL227 or vehicle control twice a week. Tumor volumes (**A**) were measured twice a week. Data were shown as the mean volume \pm SEM from $n = 7$ mice. At day 23, tumors were harvested for measurement of weight (**B**) and for immunofluorescence (IF) staining to detect the expression of tumor-infiltrating inflammatory monocyte marker CCR2 (**C**) and endothelial cell marker CD31 (**E**). DAPI staining (blue) was used to detect nuclei. Scale bar, 100 μ m. **D**, CCR2 staining was quantified as the number of CCR2⁺ cells per 40X magnified field. **F**, CD31 staining was quantified as percentage of CD31⁺ area per region of interest. *, $P < 0.05$; **, $P < 0.01$; ***, $P < 0.001$ compared with vehicle control.

angiogenesis (Fig. 1E and F). Comparing the vehicle control and HuL227 treatment groups, HuL227 did not have an effect on cell proliferation and the amounts of TAMs, but it dramatically reduced the infiltrated CCR2⁺ inflammatory monocytes and angiogenesis. Colocalization of ENO1 staining with either CCR2⁺ (Supplementary Fig. S5) or CD31⁺ (Supplementary Fig. S6) cells were also observed. We thus suggested that targeting ENO1 could reduce the tumor burden *in vivo* by regulating TME.

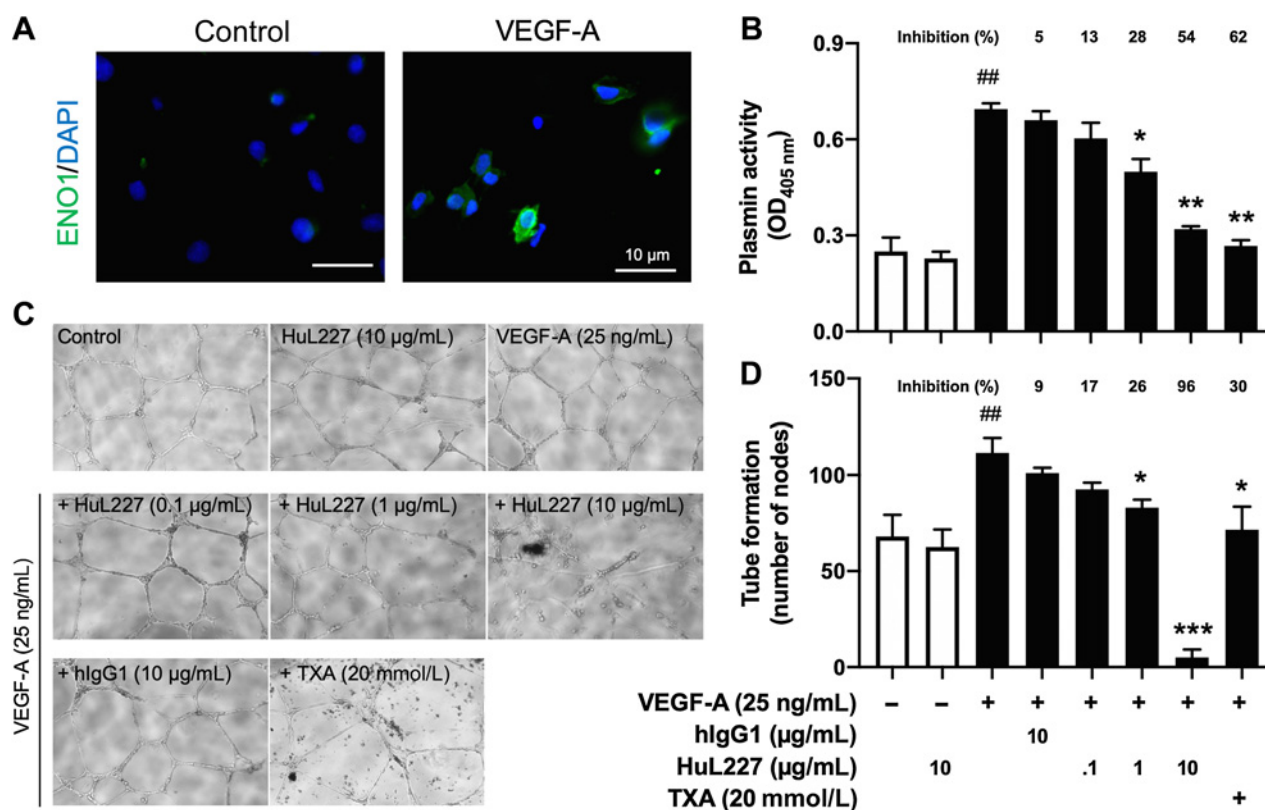
ENO1 mAb HuL227 inhibits VEGF-A-induced angiogenesis *in vitro*

To further verify the effect of HuL227 on angiogenesis, we used HUVECs for *in vitro* investigation. VEGF-A can be secreted by primary prostate cancer cells to induce cancer-associated angiogenesis (19). We found that surface ENO1 expression was relatively low or none in normal HUVECs but was increased upon VEGF-A stimulation (Fig. 2A). By inhibiting surface ENO1 as plasminogen receptor,

HuL227 dose-dependently reduced VEGF-A-induced plasmin activation (Fig. 2B). Notably, HuL227 dramatically inhibited VEGF-A-induced tube formation of HUVECs (Fig. 2C and D). These *in vitro* results were consistent with the *in vivo* finding that intratumoral CD31 expression was greatly reduced by HuL227 (Fig. 1E and F). Of note, these inhibitory effects are ENO1-dependent and probably also plasmin-associated based on the similar results obtained from TXA treatment, which binds to plasminogen and prevents plasmin activation (20). Antiangiogenesis activities were suggested to be one of the anticancer mechanisms of HuL227 to attenuate the primary prostate cancer progression.

ENO1 mAb HuL227 inhibits inflammation-induced migration and plasmin activation in androgen-independent prostate cancer cells

Ample studies clearly indicated that chronic inflammation has synergistic relationship with high-grade prostate cancer leading


Figure 2.

Anti-ENO1 mAb HuL227 inhibits VEGF-A-induced plasmin activation and tube formation in HUVEC cells. After VEGF-A stimulation for 4 hours, surface ENO1 (green) was examined by IF staining (A). DAPI staining (blue) was used to detect nuclei. Scale bar, 10 μm. B, Plasmin activation was determined by fibrinolytic assay after VEGF-A stimulation for 4 hours in the absence or presence of indicated concentrations of control hIgG1, HuL227, and TXA. Inhibition of plasmin activity (%) compared with the VEGF-A stimulation only was described. C, HUVEC cells grown on matri-gel were treated with VEGF-A for 24 hours to examine the formation of capillary-like tubes which was quantified as manual counting of nodes. D, Inhibition of tube formation (%) compared with the VEGF-A stimulation only was described. Results were shown as mean ± SD. ##*P* < 0.01 compared with untreated cells. **P* < 0.05; ***P* < 0.01; ****P* < 0.001 compared with VEGF-A-treated cells.

ultimately to metastatic spread (21). We treated two commonly used prostate cancer cell lines LNCap (androgen-dependent) and PC-3 (androgen-independent) with inflammatory stimuli, such as TNFα, which is elevated in patients with prostate cancer and also correlates to worse outcome (22). Compared with LNCap cells (Fig. 3A), higher migration abilities acquired after TNFα stimulation were detected in PC-3 cells (Fig. 3B). The IC₅₀ of HuL227 for TNFα-induced migration of PC-3 cells is measured as 2.2 μg/mL (Fig. 3C). Similar results of migration induction and inhibition were found in response to LPS stimulation in PC-3 cells but not in LNCap cells (Supplementary Fig. S7). In addition to PC-3 cells, another androgen-independent prostate cancer cell line DU145 was used to verify the effect of HuL227 on migration (Supplementary Fig. S8). The IC₅₀ of HuL227 for TNFα-induced migration was 2.5 μg/mL for DU145 cells (Fig. 3D). Consistently, HuL227 inhibits TNFα-induced plasmin activation in both PC-3 and DU145 cells with the IC₅₀ of 2.8 and 2.7 μg/mL, respectively (Fig. 3E and F). Surface expression of ENO1 was increased in PC-3 cells and DU145 upon TNFα stimulation, presumably leading to the increase of plasmin activity (Fig. 3G). Although surface ENO1 expression was also increased in LNCap cells upon LPS stimulation (Supplementary Fig. S9), the differences in acquired migration ability of PC-3 and LNCap cells after TNFα (or LPS) induction, were previously reported due to different expression levels of proinvasive molecules, such as integrin and uPAR, which were preferentially expressed in

PC-3 but not in LNCap cells (23). These results suggested that targeting ENO1 could be of potential to inhibit the ENO1/plasmin-induced spreading of androgen-independent prostate cancer cells, similar to the case of CRPC.

ENO1 mAb HuL227 attenuates tumor growth and osteoclast activity in PC-3 intratibial xenograft models

Prostate cancer frequently metastasizes to bone. We next tried to investigate the anticancer effects of HuL227 in bone TME by using a xenograft model in which PC-3 cells were inoculated into the mouse tibia. Results of hematoxylin and eosin (H&E) staining showed less tumor growth and more intact bone structures in the HuL227 treatment group when compared with the vehicle control (Fig. 4A). By using fluorescent matrix metalloproteinase (MMP) substrates as *in vivo* tracer, the tumor growth inside the bone was quantified by FMT imaging. A trend of reduction of tumor progression as assessed by MMP activity was found in the HuL227-treated group (Fig. 4B). Better imaging-based measurement, such as MRI or X-ray, would be needed to verify these results. Tumor progression-associated osteoclast activity (cathepsin K) were also monitored by *in vivo* FMT imaging of fluorescent cathepsin K substrates as tracer. We found a time-dependent increment of osteoclast activity, which could be significantly reduced by HuL227 (Fig. 4C). The suppression of osteoclast activities was thus suggested to be involved in the anticancer

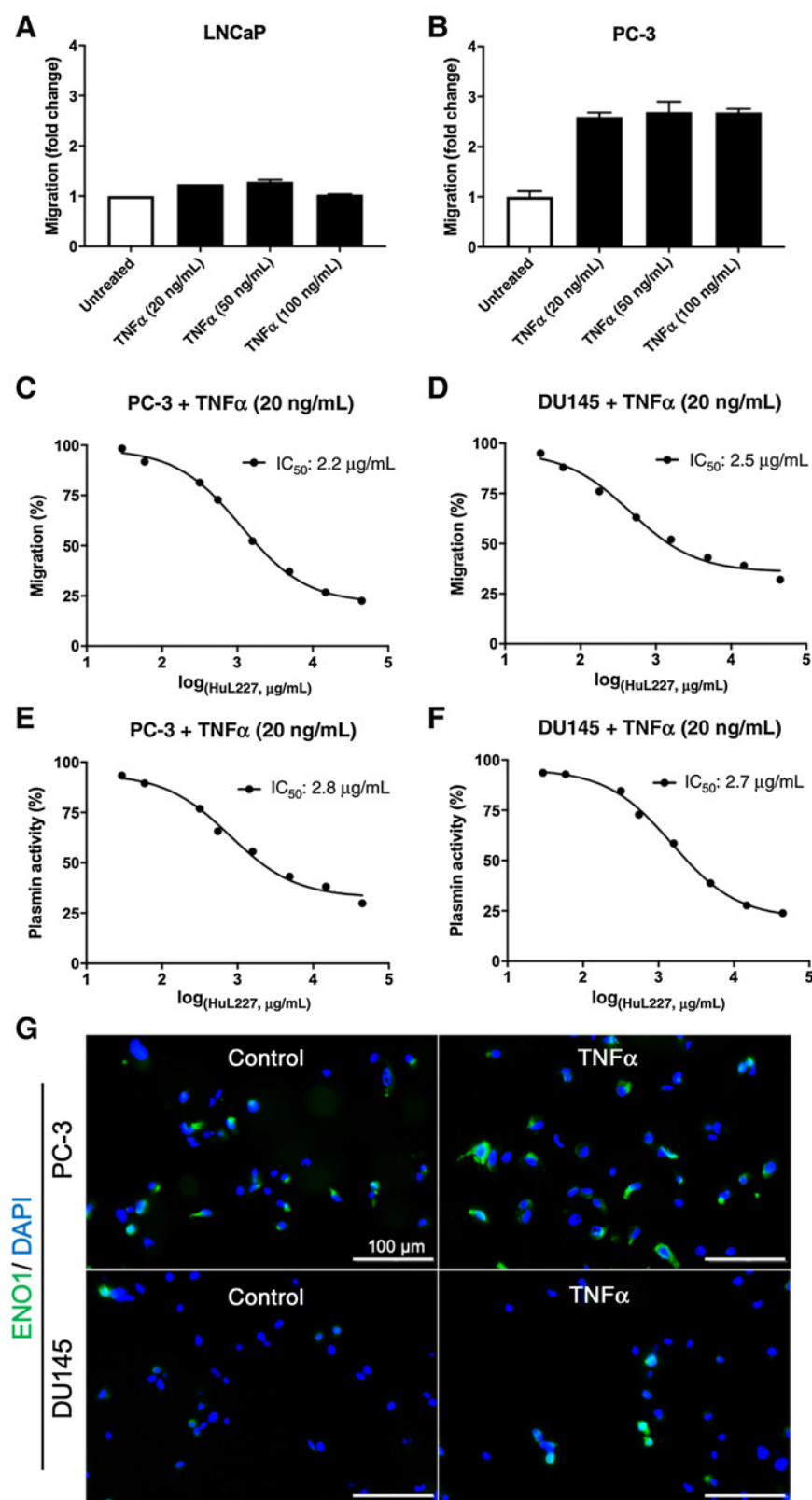
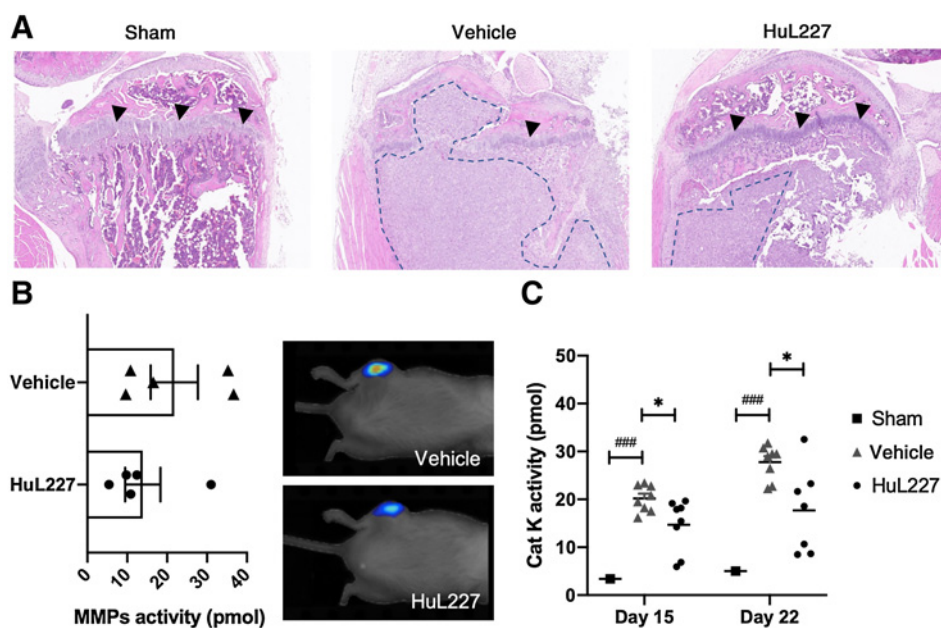


Figure 3.

Anti-ENO1 mAb HuL227 reduces inflammation-induced migration and plasmin activation in androgen-independent prostate cancer PC-3 and DU145 cells. Human prostate cancer cell lines, androgen-dependent LNCaP cells (A), or androgen-independent PC-3 cells (B) were stimulated with indicated concentrations of TNF α for 4 hours and allowed to migrate for an additional 18 hours using the transwell method. The change of migration after TNF α treatment was compared with the untreated as fold change. IC₅₀ of HuL227 for migration (C, D), and plasmin activation (E, F) was determined in TNF α -stimulated PC-3 (C, E) and DU145 (D, F) cells. IC₅₀, the concentration of an inhibitor where the response is reduced by half. G, After TNF α stimulation for 4 hours, surface ENO1 (green) was examined by IF staining. DAPI staining (blue) was used to detect nuclei. Scale bar, 100 μ m.


Figure 4.

Anti-ENO1 mAb HuL227 attenuates tumor growth and osteoclast activation in prostate cancer PC-3 intratibial xenograft model. Male NOD-SCID mice were intratibially implanted with PC-3 cells for 3 days, randomized, and dosed with 30 mg/kg anti-ENO1 mAb HuL227 or vehicle control twice a week. **A**, Dashed outlines in the representative H&E staining indicated the boundary of PC-3 tumor growth in the bone lesion on day 28. Arrow heads indicated cartilages of the bone growth plate. **B**, MMP activity was measured on day 27 by using *in vivo* tracer of MMPs substrate to semiquantify tumor volume in bone. Data were shown as the mean fluorescence intensity (pmol) \pm SEM from $n = 5$ mice. Representative images for each group were shown. **C**, Osteoclast activity (cathepsin K) was measured on day 15 and 22 by using *in vivo* tracer of cathepsin K substrate. Data were shown as the mean fluorescence intensity (pmol) \pm SEM from $n = 8$ mice, except sham $n = 1$ for background. ###, $P < 0.001$; *, $P < 0.05$. Cat K, cathepsin K.

mechanisms of HuL227 to attenuate prostate cancer progression in the bone, but the mechanism might be limited to certain type of prostate cancer. We performed a similar experiment in DU145 intratibial xenograft model (Supplementary Fig. S10), and found no significant effects of HuL227 on the osteoclast activity and tumor growth. We did see a trend, not statistically significant, of reduction in the serum levels of calcium by HuL227, which might indicate certain osteoclast activity suppression (Supplementary Fig. S10B). Nevertheless, because DU145 (osteoblastic and derived from a brain metastasis) is different from PC-3 (osteolytic and derived from a bone metastasis) by their origins, we suggested that the different natures of DU145 and PC3 could result in different responses to HuL227 in the bone microenvironment.

ENO1 mAb HuL227 reduces inflammation-enhanced osteoclast activity and prometastatic cytokines secretion from osteoclasts

Inflammation has long been known to contribute to osteolysis and debilitating skeletal instability in cancer (24). We therefore pretreated Raw264.7 cells (mouse monocyte) with $\text{TNF}\alpha$, and the cells were allowed to differentiate to osteoclasts in response to the stimulation of receptor activator of nuclear factor kappa-B ligand (RANKL; ref. 25). HuL227 treatment could dose-dependently reduce the activation of plasmin (Supplementary Fig. S11) and the expression of osteoclast-specific genes *NFATC1* (Fig. 5A) and *CTSK* (Fig. 5B). The latter suggested monocyte-derived osteoclast-specific gene expression could be inhibited by HuL227 in an inflammatory TME. To further delineate the regulation of HuL227 on the functional roles of osteoclasts in prostate cancer bone metastasis, we treated Raw264.7-derived osteoclasts with $\text{TNF}\alpha$ to mimic inflammatory bone TME. HuL227 treatment was able to inhibit secretion of prometastatic chemokine CCL2

(Fig. 5C) and cytokine $\text{TGF}\beta$ (Fig. 5D) by osteoclasts in a dose-dependent manner. Taken together, HuL227 was able to inhibit the expression of osteoclast-specific genes presumably derived from monocytes and their following ENO1-dependent and plasmin-associated protumor and proinvasive roles in the TME *in vitro*.

ENO1 mAb HuL227 reduces CCL2 or $\text{TGF}\beta$ -enhanced cell migration of androgen-independent PC-3 and DU145 cells

We have already shown that HuL227 could inhibit inflammation-enhanced migration of androgen-independent prostate cancer cells, which was ENO1-dependent and plasmin-associated. In prostate cancer bone metastasis, osteoclast-secreted CCL2 and $\text{TGF}\beta$ are key mediators of attracting and activating primary cancer cells migrating to the bone (3). Therefore, the chemotaxis and migration abilities of PC-3 and DU145 were measured to mimic inflammatory bone TME involving CCL2 and $\text{TGF}\beta$. Both prostate cells were pretreated with $\text{TNF}\alpha$ and allowed to migrate in response to the gradient of CCL2. This inflammation-enhanced chemotaxis was significantly reduced by HuL227 (or TXA) treatment in a dose-dependent manner in both cell types (Fig. 6A and B). Similarly, $\text{TGF}\beta$ -induced migration of PC-3 (Fig. 6C) and DU145 (Fig. 6D) was also inhibited by HuL227 (or TXA) treatment. In addition, the inflammatory TME would affect the circulating monocytes to favor prostate cancer bone metastasis, which was crucial to facilitate the process of bone metastasis (26). We used a monocyte cell line THP-1 to examine the effects of HuL227 on the inflammation-enhanced cell migration/chemotaxis. HuL227 could inhibit $\text{TNF}\alpha$ -induced migration of monocytes in a dose-dependent manner, and similar inhibitory effect of HuL227 was also obtained for monocyte migration in response to a CCL2 gradient (Supplementary

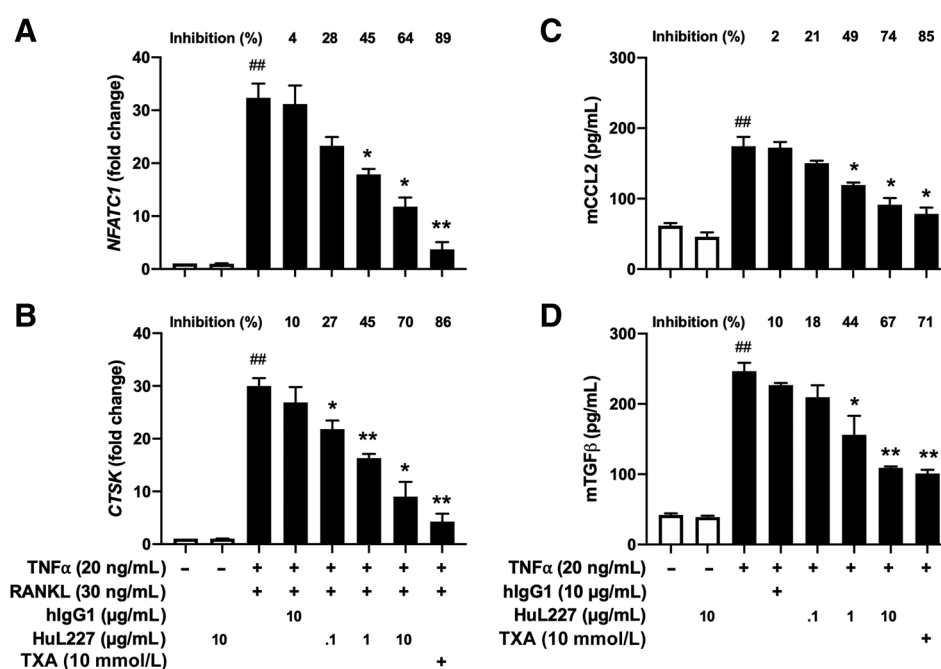


Figure 5.

Anti-ENO1 mAb HuL227 reduces inflammation-enhanced activation and secretion of prometastatic cytokines in Raw 264.7-derived osteoclasts. Raw 264.7 cells were pre-treated with TNF α for 4 hours and added RANKL for 4 days in the absence or presence with indicated concentrations of HuL227, 10 μ g/mL hlgG1, and 10 mmol/L TXA. To measure osteoclast activation, osteoclast-specific genes *NFATC1* (**A**) and *CTSK* (cathepsin K; **B**) mRNA expression were determined by reverse transcription followed by real-time qPCR. Inhibition of induced gene expression (%) compared with the nontreatment was described. Raw264.7-differentiated osteoclasts were stimulated with TNF α in the absence or presence with indicated concentrations of HuL227, 10 μ g/mL hlgG1, and 10 mmol/L TXA for 24 hours. Supernatant was collected for determination of murine CCL2 (**C**) and TGF β (**D**) levels by ELISA. Inhibition of induced cytokine production (%) compared with the nontreatment was described. ##, $P < 0.01$ compared with untreated cells. *, $P < 0.05$; **, $P < 0.01$ compared with the cytokine-stimulated cells. mCCL2, murine CCL2; mTGF β , murine TGF β .

Fig. S12). The results were in agreement with Fig. 1C and D. Taken together, this study suggested that a novel ENO1 mAb could enable a feasible strategy to tackle multiple interacting players, prostate cancer cells, endothelial cells, osteoclasts, and monocytes via a common molecular target, in the complicating prostate cancer progression and bone metastasis (Fig. 6E).

Discussion

ADT, including surgical or medical castration, antiandrogens, and androgen biosynthesis inhibitors, is highly effective and used as the standard first-line treatment for patients with advanced prostate cancer. However, despite its initial response, ADT rarely cures the cancer itself, and CRPC almost always recurs within 18 to 24 months due to various mechanisms such as androgen receptor (AR) mutations, amplification, or splice variants (27). New AR-targeted therapies, such as enzalutamide and abiraterone, and a chemotherapy agent, cabazitaxel, have been approved for treating patients with CRPC (28–30). Unfortunately, all patients with CRPC eventually evade AR-targeted therapy, and mCRPC ultimately develops as CRPC progresses and metastasizes (31). Patients with mCRPC have a predicted survival rate of fewer than 2 years, and more than 90% of patients are developing bone metastases (32). Three emerging areas of therapeutic approaches have been pursued for mCRPC, including immunotherapy (particularly immune checkpoint blockers), PARP inhibitors, and prostate-specific membrane antigen (PSMA)-targeted modalities (33). Conceptually in agreement to these approaches but with broader mechan-

isms, we hypothesized that targeting ENO1 on both cancer cells and TME would provide more efficacious benefits for mCRPC outcome.

Here, for the first time, we show that a first-in-class anti-ENO1 mAb might be deployed as a potential anti-mCRPC therapy. Given the heterogeneity of mCRPC, it would be very difficult to identify a single molecular target commonly shared by multiple players in the complicated process of prostate cancer progression and bone metastasis, which could involve primary tumor, stroma, metastatic milieu, and even immune components. This ENO1 mAb could intercept key players involved in the seed-to-soil path (34) by inhibiting the fundamental migration capability and accompanied biological activities of various cell types, including androgen-independent prostate cancer cells as well as the constituents of TME (endothelial cells, osteoclasts, and monocytes; summarized in Fig. 6E). We next discussed the possible mechanism of actions by which ENO1 mAb might serve the need of a treatment option for prostate cancer progression and bone metastasis.

For the antiangiogenesis activities of HuL227, we found there was a dramatic reduction in VEGF-A-induced tube formation of HUVECs when treated with HuL227 at the concentration of 10 μ g/mL (~68 nmol/L). *In vivo* studies also showed consistent results that HuL227 could reduce intratumoral angiogenesis in PC-3 subcutaneous xenograft model. Because only one angiogenesis marker CD31 was used for the *in vivo* study, additional evidence should be obtained in the future study. The possible mechanism of this antiangiogenesis effect of HuL227 is unclear. However, a plasmin-associated regulation may be speculated because plasmin was also shown to play a critical role in

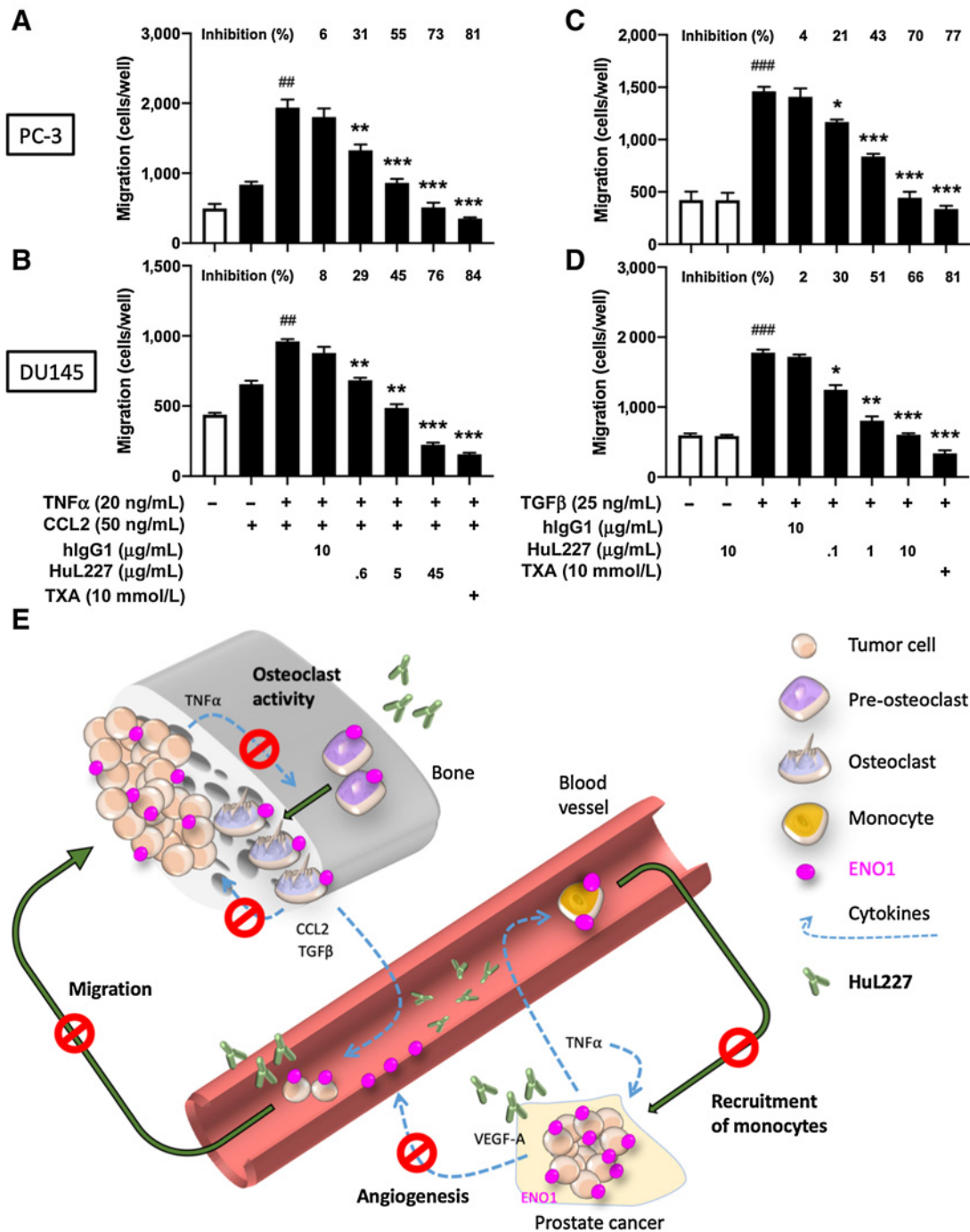


Figure 6. Anti-ENO1 mAb HuL227 reduces inflammation-enhanced chemotaxis and migration in androgen-independent prostate cancer PC-3 and DU145 cells. In CCL2-chemotaxis assay, PC-3 (A) or DU145 (B) were pretreated with TNF α for 4 hours and allowed to migrate toward chemoattractant CCL2 in the absence or presence with indicated concentrations of HuL227, 10 μ g/mL human IgG1, and 10 mmol/L TXA for an additional 18 hours. Inhibition of migration (%) compared with the nontreatment was described. In migration assay, PC-3 (C) or DU145 (D) were treated with TGF β and allowed to migrate in the absence or presence with indicated concentrations of HuL227, 10 μ g/mL hlgG1, and 10 mmol/L TXA for 18 hours. ##, $P < 0.01$; ###, $P < 0.001$ compared with untreated cells. *, $P < 0.05$; **, $P < 0.01$; ***, $P < 0.001$ compared with cytokine-stimulated cells. **E**, Putative action mechanisms of HuL227 in prostate cancer. ENO1 was a molecular target commonly shared by prostate cancer cells, monocytes, osteoclasts, and endothelium cells in advanced prostate cancer TME. All these ENO1-expressing cells are crucial for the progressing of advanced prostate cancer to bone metastasis. HuL227 was hypothesized to inhibit the migration and invasion of prostate cancer cells from prostate to blood vessel and ultimately to bone. The induction effects of essential mediators, such as CCL2, TGF β , and TNF α , to drive this migration and invasion process could also be inhibited by HuL227. The angiogenesis crucial for tumor growth can be inhibited by HuL227 in prostate cancer as well.

promoting the binding of VEGF to the VEGF receptor by cleavage and release of the VEGF receptor recognition domain of VEGF (35). TXA is a lysine analogue developed to saturate the lysine binding sites of plasminogen and thus prevent plasmin formation (20). Our data also showed that TXA could inhibit tube formation of HUVEC cells. Combining the evidence that blockade of VEGF inhibits the growth of human prostate cancer via suppression of angiogenesis in preclinical studies (36), the action mechanism of HuL227 in treating prostate cancer might be reasoned accordingly. In addition, plasmin is also known to activate lymphangiogenic factors VEGF-C and VEGF-D (37). Whether HuL227 affects lymphangiogenesis in the context of prostate cancer metastasis awaits further investigation. To our knowledge, this is the first time that surface ENO1 has been directly shown to be essential for angiogenesis.

Chronic inflammation has been widely accepted to promote the development and progression of prostate cancer, in which the inflammatory cytokine-rich TME provides essential signaling for EMT and angiogenesis (5). In patients with prostate cancer, significantly elevated serum levels of TNF α were found in metastatic disease compared with localized disease (22), which correlates to shorter survival time (38). Although high doses of TNF α are known to induce cell apoptosis, low doses of TNF α could induce angiogenesis, proliferation, invasion, and metastasis of tumor cells (39). In this study, we are the first to demonstrate that targeting surface ENO1 would suppress prostate cancer migration, monocyte chemotaxis, and osteoclast activity in the context of TNF α stimulation. ENO1 externalization upon stimuli, such as TGF β , CCL2, and TNF α , was shown in breast cancer cells (40) and LPS-treated lung cancer cells (41). It is a reasonable assumption that ENO1 mAb could have therapeutic potential in these types of cancer as well when inflammation plays a tumor-promoting role.

In the TME of bone, accelerated bone resorption promotes the release of bone-derived growth factors such as TGF β to further facilitate the progression of prostate cancer (42). ENO1 mAb HuL227 not only reduces TGF β secretion from the osteoclasts, but also significantly inhibits TGF β -induced migration of the prostate cancer cells. *In vivo* evidence is still needed to verify this mechanism. We speculated that HuL227 inhibits TGF β secretion via a plasmin-dependent pathway, which was supported by our observation that TXA had a similar inhibitory effect. It has been reported that plasmin is able to regulate the activation of cell-associated latent form of TGF β in a bleomycin-induced lung injury animal model (43). One report showed that blockade of TGF β signaling promoted phenotypic conversion of EMT to mesenchymal-epithelial transition (MET), leading to redifferentiation of prostate tumors *in vivo* (44). Although we didn't observe such phenotypic changes when prostate cancer cells were cotreated with TGF β and ENO1 mAb, it remained to be addressed whether HuL227 could regulate EMT signaling. Ample studies showed silencing of ENO1 reduced either EMT-related genes or proteins, for example, in glioma (45) and endometrial carcinoma (46), which might be partly due to the inhibition of intracellular function of ENO1 as a glycolytic enzyme. In contrast, HuL227 is mainly to block ENO1 as a plasminogen receptor based on current evidence and thus different from genetic knockdown of ENO1 expression.

Moreover, this is the first study to show specific targeting surface ENO1 would reduce inflammation-enhanced activation of osteoclasts. Shin and colleagues previously reported that increased expression level of ENO1 on the surface of osteoclast precursors plays a positive role in osteoclastogenesis in the context of rheumatoid arthritis (47). However, they used ENO1-targeting siRNA to downregulate overall ENO1 expression, which is quite different from our antibody approach to target solely at surface ENO1. We believe by targeting surface ENO1, HuL227 would disrupt prostate cancer-mediated osteoclast activation

and osteolysis, which is in agreement with the reported contributions of plasminogen and plasmin in bone metabolism (48). Because we have obtained different results between the PC-3 (osteolytic) and DU145 (osteoblastic) intratibial xenograft models, the effects of HuL227 on osteoblasts and its homeostasis with osteoclasts remained to be investigated in the metastasis of prostate cancer to bone. Furthermore, we have shown that HuL227 could inhibit chemotaxis and migration of monocytes, the precursor of osteoclast. The role of CCL2/CCR2 axis for inflammatory monocytes recruitment is not clear in prostate cancer, but it has been shown to promote breast cancer bone metastasis (49). Although HuL227 could not reduce TAMs as a whole (measured by F4/80⁺) in the subcutaneous PC-3 xenograft, we find HuL227 significantly reduced the recruitment of CCR2⁺ inflammatory monocytes. Monocytes were previously shown to induce prostate cancer cell invasion (50). In addition, we are currently looking into the surface ENO1-expressing subpopulations of TAMs in prostate cancer, given the highly heterogeneous populations of macrophages.

In conclusion, this study demonstrated that ENO1 could be a valuable target commonly shared by essential interacting components in the complex metastatic progression of primary prostate cancer to bone. Due to the multifaceted roles of ENO1 in such complex process, only some antitumor properties of the ENO1 mAb HuL227 were identified so far. Considering such a complex process from primary tumor to bone metastasis, our finding on the role of ENO1 is limited by the experimental setting, but these evidences certainly justify further investigation in the animal model more representing bone metastasis. In the full picture of prostate cancer advancing to bone, it is conceivable, but remained to be proven, that blocking ENO1 would attenuate fundamental mobility and migration of essential cell players in a plasmin-dependent manner, by which was crucial for netting interactive *milieu* containing but not limited to chemokines and cytokines in order to construct a protumor TME for extravasation, seeding, and growing tumor. Based on our results, we believe HuL227 is worth further investigation to justify its clinical development to tackle mCRPC.

Authors' Disclosures

T.-T. Yuan reports patents for Alpha-Enolase Specific Antibodies and Methods of Uses in Cancer Therapy, Humanized Alpha-Enolase Specific Antibodies and Methods of Uses In Cancer Therapy, and Antibodies Specific to Alpha-Enolase and Uses Thereof issued. No disclosures were reported by the other authors.

Authors' Contributions

M.-L. Chen: Data curation, validation, investigation, methodology. **T.-T. Yuan:** Conceptualization, supervision, funding acquisition, writing-review and editing. **C.-F. Chuang:** Data curation, methodology. **Y.-T. Huang:** Data curation, methodology. **I.-C. Chung:** Data curation, methodology, writing-original draft. **W.-C. Huang:** Conceptualization, writing-original draft, project administration, writing-review and editing.

Acknowledgments

The authors would like to thank TFBS Bioscience and Trineo Biotechnology for their assistance with the *in vivo* studies during the development of ENO1 mAb HuL227. All work was fully funded by HuniLife Biotechnology.

The publication costs of this article were defrayed in part by the payment of publication fees. Therefore, and solely to indicate this fact, this article is hereby marked "advertisement" in accordance with 18 USC section 1734.

Note

Supplementary data for this article are available at Molecular Cancer Therapeutics Online (<http://mct.aacrjournals.org/>).

Received March 29, 2021; revised August 11, 2021; accepted June 3, 2022; published first June 14, 2022.

References

- Siegel RL, Miller KD, Jemal A. Cancer statistics, 2020. *CA Cancer J Clin* 2020;70:7–30.
- Chen X, Li Q, Liu X, Liu C, Liu R, Rycaj K, et al. Defining a population of stem-like human prostate cancer cells that can generate and propagate castration-resistant prostate cancer. *Clin Cancer Res* 2016;22:4505–16.
- Adekoya TO, Richardson RM. Cytokines and chemokines as mediators of prostate cancer metastasis. *Int J Mol Sci* 2020;21:4449.
- Barron DA, Rowley DR. The reactive stroma microenvironment and prostate cancer progression. *Endocr Relat Cancer* 2012;19:R187–204.
- Stark T, Livas L, Kyprianou N. Inflammation in prostate cancer progression and therapeutic targeting. *Transl Androl Urol* 2015;4:455–63.
- Zhang X. Interactions between cancer cells and bone microenvironment promote bone metastasis in prostate cancer. *Cancer Commun* 2019;39:76.
- Ottewill PD. The role of osteoblasts in bone metastasis. *J Bone Oncol* 2016;5:124–7.
- Nishizawa S, Inagaki T, Iba A, Kikkawa K, Kodama Y, Matsumura N, et al. Zoledronic acid prevents decreases in bone mineral density in patients with prostate cancer undergoing combined androgen blockade. *Springerplus* 2014;3:586.
- Aisina RB, Mukhametova LI. [Structure and functions of plasminogen/plasmin system]. *Bioorg Khim* 2014;40:642–57.
- Wygreccka M, Marsh LM, Morty RE, Henneke I, Guenther A, Lohmeyer J, et al. Enolase-1 promotes plasminogen-mediated recruitment of monocytes to the acutely inflamed lung. *Blood* 2009;113:5588–98.
- Diaz-Ramos A, Roig-Borrellas A, Garcia-Melero A, Lopez-Aleman R. alpha-Enolase, a multifunctional protein: its role on pathophysiological situations. *J Biomed Biotechnol* 2012;2012:156795.
- Bae S, Kim H, Lee N, Won C, Kim HR, Hwang YI, et al. alpha-Enolase expressed on the surfaces of monocytes and macrophages induces robust synovial inflammation in rheumatoid arthritis. *J Immunol* 2012;189:365–72.
- Capello M, Ferri-Borgogno S, Cappello P, Novelli F. Alpha-enolase: a promising therapeutic and diagnostic tumor target. *FEBS J* 2011;278:1064–74.
- Hsiao KC, Shih NY, Fang HL, Huang TS, Kuo CC, Chu PY, et al. Surface alpha-enolase promotes extracellular matrix degradation and tumor metastasis and represents a new therapeutic target. *PLoS One* 2013;8:e69354.
- Principe M, Ceruti P, Shih NY, Chattaragada MS, Rolla S, Conti L, et al. Targeting of surface alpha-enolase inhibits the invasiveness of pancreatic cancer cells. *Oncotarget* 2015;6:11098–113.
- Wang L, Qu M, Huang S, Fu Y, Yang L, He S, et al. A novel alpha-enolase-targeted drug delivery system for high efficacy prostate cancer therapy. *Nanoscale* 2018;10:13673–83.
- Yu L, Shi J, Cheng S, Zhu Y, Zhao X, Yang K, et al. Estrogen promotes prostate cancer cell migration via paracrine release of ENO1 from stromal cells. *Mol Endocrinol* 2012;26:1521–30.
- Rabbani SA, Ateeq B, Arakelian A, Valentino ML, Shaw DE, Dauffenbach LM, et al. An anti-urokinase plasminogen activator receptor antibody (ATN-658) blocks prostate cancer invasion, migration, growth, and experimental skeletal metastasis in vitro and in vivo. *Neoplasia* 2010;12:778–88.
- Roberts E, Cossigny DA, Quan GM. The role of vascular endothelial growth factor in metastatic prostate cancer to the skeleton. *Prostate Cancer* 2013;2013:418340.
- Markus G, Priore RL, Wissler FC. The binding of tranexamic acid to native (Glu) and modified (Lys) human plasminogen and its effect on conformation. *J Biol Chem* 1979;254:1211–6.
- Gurel B, Lucia MS, Thompson IM Jr, Goodman PJ, Tangen CM, Kristal AR, et al. Chronic inflammation in benign prostate tissue is associated with high-grade prostate cancer in the placebo arm of the prostate cancer prevention trial. *Cancer Epidemiol Biomarkers Prev* 2014;23:847–56.
- Michalaki V, Syrigos K, Charles P, Waxman J. Serum levels of IL-6 and TNF-alpha correlate with clinicopathological features and patient survival in patients with prostate cancer. *Br J Cancer* 2004;90:2312–6.
- Lim HW, Hong S, Jin W, Lim S, Kim SJ, Kang HJ, et al. Up-regulation of defense enzymes is responsible for low reactive oxygen species in malignant prostate cancer cells. *Exp Mol Med* 2005;37:497–506.
- Abu-Amer Y. Inflammation, cancer, and bone loss. *Curr Opin Pharmacol* 2009;9:427–33.
- Luo G, Li F, Li X, Wang ZG, Zhang B. TNFalpha and RANKL promote osteoclastogenesis by upregulating RANK via the Nf-kappaB pathway. *Mol Med Rep* 2018;17:6605–11.
- Cavassani KA, Meza RJ, Habel DM, Chen JF, Montes A, Tripathi M, et al. Circulating monocytes from prostate cancer patients promote invasion and motility of epithelial cells. *Cancer Med* 2018;7:4639–49.
- Seruga B, Ocana A, Tannock IF. Drug resistance in metastatic castration-resistant prostate cancer. *Nat Rev Clin Oncol* 2011;8:12–23.
- Scher HI, Fizazi K, Saad F, Taplin ME, Sternberg CN, Miller K, et al. Increased survival with enzalutamide in prostate cancer after chemotherapy. *N Engl J Med* 2012;367:1187–97.
- Ryan CJ, Smith MR, de Bono JS, Molina A, Logothetis CJ, de Souza P, et al. Abiraterone in metastatic prostate cancer without previous chemotherapy. *N Engl J Med* 2013;368:138–48.
- de Bono JS, Oudard S, Ozguroglu M, Hansen S, Machiels JP, Kocak I, et al. Prednisone plus cabazitaxel or mitoxantrone for metastatic castration-resistant prostate cancer progressing after docetaxel treatment: a randomised open-label trial. *Lancet* 2010;376:1147–54.
- Bluemn EG, Coleman IM, Lucas JM, Coleman RT, Hernandez-Lopez S, Tharakan R, et al. Androgen receptor pathway-independent prostate cancer is sustained through FGF signaling. *Cancer Cell* 2017;32:474–89.
- Huang X, Chau CH, Figg WD. Challenges to improved therapeutics for metastatic castrate resistant prostate cancer: from recent successes and failures. *J Hematol Oncol* 2012;5:35.
- Marshall CH, Antonarakis ES. Emerging treatments for metastatic castration-resistant prostate cancer: immunotherapy, PARP inhibitors, and PSMA-targeted approaches. *Cancer Treat Res Commun* 2020;23:100164.
- Morgan SC, Parker CC. Local treatment of metastatic cancer—killing the seed or disturbing the soil? *Nat Rev Clin Oncol* 2011;8:504–6.
- Roth D, Piekarek M, Paulsson M, Christ H, Bloch W, Krieg T, et al. Plasmin modulates vascular endothelial growth factor-A-mediated angiogenesis during wound repair. *Am J Pathol* 2006;168:670–84.
- Sarkar C, Goswami S, Basu S, Chakraborty D. Angiogenesis inhibition in prostate cancer: An update. *Cancers* 2020;12:2382.
- McCull BK, Baldwin ME, Roufail S, Freeman C, Moritz RL, Simpson RJ, et al. Plasmin activates the lymphangiogenic growth factors VEGF-C and VEGF-D. *J Exp Med* 2003;198:863–8.
- Nakashima J, Tachibana M, Ueno M, Miyajima A, Baba S, Murai M. Association between tumor necrosis factor in serum and cachexia in patients with prostate cancer. *Clin Cancer Res* 1998;4:1743–8.
- Wang X, Lin Y. Tumor necrosis factor and cancer, buddies or foes? *Acta Pharmacol Sin* 2008;29:1275–88.
- Didiasova M, Zakrzewicz D, Magdolen V, Nagaraj C, Balint Z, Rohde M, et al. STIM1/ORAI1-mediated Ca²⁺ influx regulates Enolase-1 exteriorization. *J Biol Chem* 2015;290:11983–99.
- Zakrzewicz D, Didiasova M, Kruger M, Giaimo BD, Borggreffe T, Mieth M, et al. Protein arginine methyltransferase 5 mediates enolase-1 cell surface trafficking in human lung adenocarcinoma cells. *Biochim Biophys Acta Mol Basis Dis* 2018;1864:1816–27.
- Berish RB, Ali AN, Telmer PG, Ronald JA, Leong HS. Translational models of prostate cancer bone metastasis. *Nat Rev Urol* 2018;15:403–21.
- Khalil N, Corne S, Whitman C, Yacyshyn H. Plasmin regulates the activation of cell-associated latent TGFβ1 secreted by rat alveolar macrophages after in vivo bleomycin injury. *Am J Respir Cell Mol Biol* 1996;15:252–9.
- Paller C, Pu H, Begemann DE, Wade CA, Hensley PJ, Kyprianou N. TGF-β receptor I inhibitor enhances response to enzalutamide in a pre-clinical model of advanced prostate cancer. *Prostate* 2019;79:31–43.
- Song Y, Luo Q, Long H, Hu Z, Que T, Zhang X, et al. Alpha-enolase as a potential cancer prognostic marker promotes cell growth, migration, and invasion in glioma. *Mol Cancer* 2014;13:65.
- Zhao M, Fang W, Wang Y, Guo S, Shu L, Wang L, et al. Enolase-1 is a therapeutic target in endometrial carcinoma. *Oncotarget* 2015;6:15610–27.
- Shin JH, Song JE, Park JS, Shon SH, Lee EY, Lee EB, et al. AB0071 Alpha-enolase expression on the cell surface of osteoclast precursors plays a positive role in osteoclastogenesis of monocyte/macrophage in Rheumatoid Arthritis. *Ann Rheum Dis* 2016;75:921.
- Kanno Y, Ishisaki A, Kawashita E, Chosa N, Nakajima K, Nishihara T, et al. Plasminogen/plasmin modulates bone metabolism by regulating the osteoblast and osteoclast function. *J Biol Chem* 2011;286:8952–60.
- Ma RY, Zhang H, Li XF, Zhang CB, Selli C, Tagliavini G, et al. Monocyte-derived macrophages promote breast cancer bone metastasis outgrowth. *J Exp Med* 2020;217:e20191820.
- Lindholm PF, Sivapurapu N, Jovanovic B, Kajdacsy-Balla A. Monocyte-induced prostate cancer cell invasion is mediated by chemokine ligand 2 and nuclear factor-kappaB activity. *J Clin Cell Immunol* 2015;6:308.